Fuel cell electrocatalsis : oxygen reduction on Pt-based nanoparticle catalysts

Vliet, D.F. van der

Chapter 3

Monodisperse Pt_3Co Nanoparticles as a Catalyst for the Oxygen Reduction Reaction: Size-Dependent Activity

Monodisperse Pt_3Co nanoparticles with size controlled from 3 to 9 nm have been synthesized through an organic solvothermal approach and applied as electrocatalysts for the oxygen reduction reaction. Electrochemical study shows that the Pt_3Co nanoparticles are highly active for the oxygen reduction reaction and the activity is size-dependent. The optimal size for maximal mass activity was established to be around 4.5 nm by balancing the electrochemically active surface area and specific activity.

The contents of this chapter have been published: C. Wang, D. van der Vliet, K.C. Chang, H. You, D. Strmcnik, J. Schlueter, N.M. Markovic and V.R. Stamenkovic, *J. Phys. Chem. C.*, 113 **(2009)** 19365

3.1 Introduction

Alloy nanoparticles (NPs) have attracted increasing interest due to their superior performance in magnetic [1-5], optical [6-9] and catalytic [10-14] applications. Particularly, Pt alloys with transition metals (MPt with M = Fe, Co, Ni, etc.) have been found to be highly active for oxygen reduction, the troubled cathode reaction in fuel cells. [15, 16] This has initiated a lot of efforts in synthesis of Pt-based alloy catalysts, which are usually in the form of Pt_3M NPs dispersed in a high surface area carbon matrix. The approaches mostly include co-precipitation of metal salts in aqueous solution [17, 18], impregnation of transition metals into Pt/carbon catalyst [19, 20], and electrodeposition. [21] Despite the progress in preparing various types of alloy catalyst, synthesis of catalysts with monodisperse and size-controlled alloy NPs is yet challenging in the literature. On the other hand, the particle size effect is known to play an important role in catalysis, particularly in the case of electrocatalysts comprising NPs. Not only the activity but also the reaction mechanism and selectivity have been reported to be dependent on the catalyst size. [22-27] Contrary to the extensive study on conventional Pt/carbon catalysts, size-dependent activity has not been well investigated for Pt alloy catalysts [28, 29], which yet requires monodisperse alloy NPs of controlled size, composition, structure and uniform shape. [25]

3.2 Experimental

We use Pt_3Co as an example for systematic studies of size-dependent catalytic activity for the oxygen reduction reaction (ORR). Monodisperse Pt_3Co NPs were synthesized through an organic solvothermal approach modified from previous publications [30, 31], which has been demonstrated as a robust method for preparing monodisperse alloy NPs with size control and homogeneous compositions. [1-13, 32]. Electrochemical properties were compared to the commercially available state-of-the-art Pt/carbon catalyst supplied by Tanaka. Platinum acetylacetonate, $Pt(acac)_2$, was reduced by 1,2-tetradecanediol in the presence of 1-adamantanecarboxylic acid (ACA) and a large excess of oleylamine, while Co was introduced by thermal decomposition of cobalt carbonyl, $Co_2(CO)_8$ (figure 3.1a and section 3.5). Adding $Co_2(CO)_8$ at different temperatures gave $CoPt_3$

NPs of various sizes. Figure 3.1b–e show representative transmission electron microscopy (TEM) images of $CoPt_3$ NPs of 3, 4.5, 6 and 9 nm obtained by adding $Co_2(CO)_8$ at 225, 200, 170 and 145 °C, respectively. The control of size in this case has been reported to be due to a balance between the rates of nucleation and growth. [31] Energy-dispersive X-ray spectroscopy (EDX) analysis of the NPs shows the atomic ratio between Co and Pt is equal to 1:3 (figure 3.5). More experimental details are given in section 3.5.

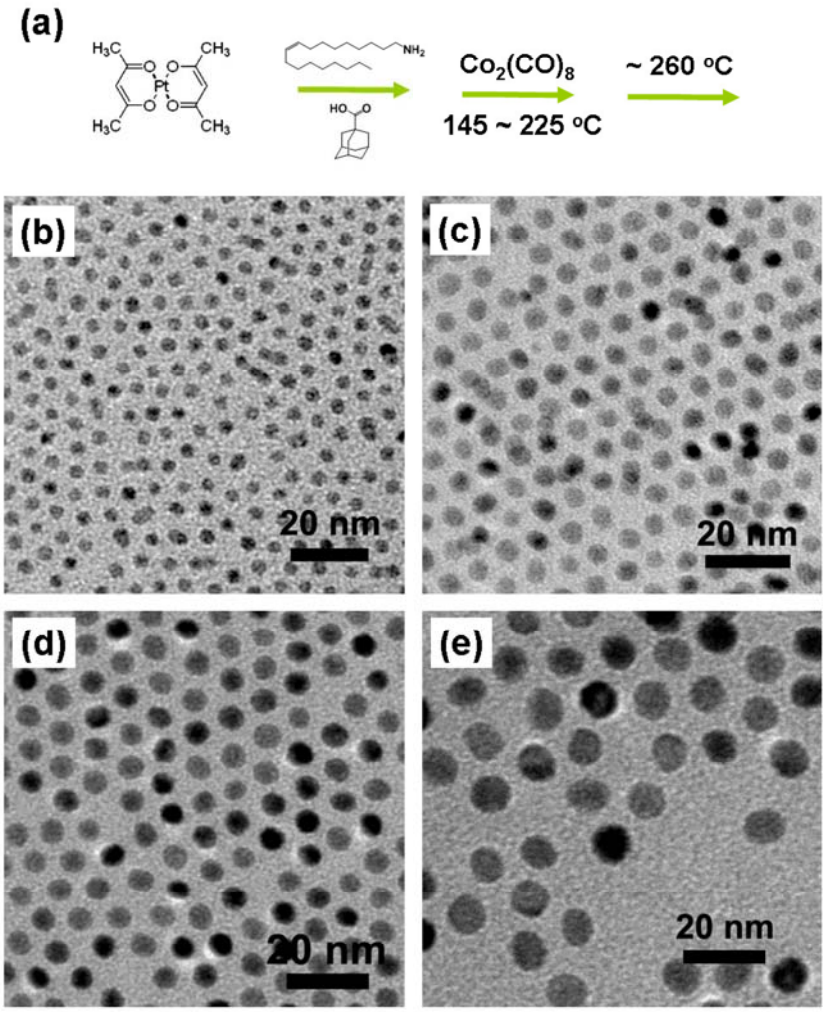

Figure 3.1. (a) Schematic illustration of the synthetic route for monodisperse $CoPt_3$ NPs. (b) - (e) TEM images of as-synthesized 3, 4.5, 6 and 9 nm $CoPt_3$ NPs.

3.3 Results and Discussion

Figure 3.2a shows X-ray diffraction (XRD) patterns of the as-synthesized $CoPt_3$ NPs. All the XRD patterns correspond to a face-centered cubic (fcc) $CoPt_3$ crystal. [30, 31] As the NP size increases, the XRD peaks become sharper; indicating the increase of crystalline size in the NPs. Crystalline sizes can further be calculated from the XRD patterns according to the Scherrer Equation, as shown in figure 3.2b. These sizes are quite close to those observed by TEM, implying the single-crystalline nature of individual NPs, which is also consistent with the high resolution TEM image analysis in the previous reports. [30, 31]

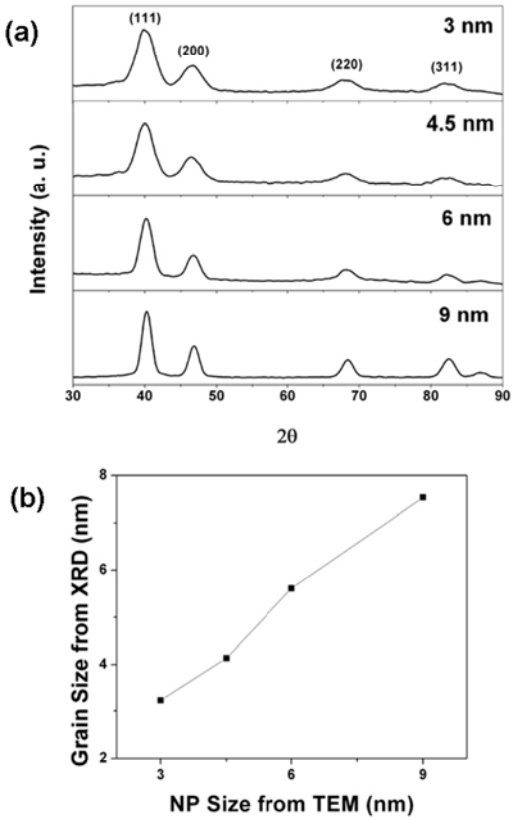

Figure 3.2. (a) XRD patterns of $CoPt_3$ NPs of various sizes showing the typical peaks of $CoPt_3$ crystals in fcc phase. (b) Crystalline sizes of $CoPt_3$ NPs as calculated from the XRD patterns according to the Scherrer Equation.

The as-synthesized NPs were supported on carbon black (Tanaka, ~ 900 m^2/g) via a colloidal-deposition approach [33] by mixing the NPs and carbon in chloroform suspension, followed by sonication. Organic surfactants were removed by heat treatment of the NPs/carbon mixture in an oxygen-containing atmosphere at 185°C. [34] The obtained catalyst was then dispersed in deionized water by vigorous sonication, and the formed suspension was pipetted on a glassy carbon (GC) electrode (6 mm in diameter). The ratio of Pt in the catalyst was tuned to 28%, and the loading of Pt on the GC electrode was controlled at 9 $\mu g/cm^2_{disk}$, with the exception of 9 nm particles, which had a loading of 12 $\mu g/cm^2_{disk}$ in order to reach the appropriate diffusion limiting current based on the disk geometry. After drying under a flow of argon, the GC electrode was immersed into 0.1 M $HClO_4$ for electrocatalytic measurements, which was carried out in a three compartment electrochemical cell with a Pt wire as counter and an Ag/AgCl as reference electrode. All potentials in this report are given versus reversible hydrogen electrode (RHE), and readout currents are corrected for the ohmic iR drop. [35, 40] The cyclic voltammogram (CV) was collected in Ar saturated solutions with a scan rate of 50 mV/s at 20°C, and ORR activity was measured by rotating disk electrode (RDE) method with a scan rate of 20 mV/s at 60°C. The electrochemical surface area of the catalyst was evaluated from the charge of under potentially deposited hydrogen (H_{upd}) and CO stripping (figure 3.6 and 3.7), and used to normalize the measured electrode current for the calculation of specific activity, which is given as the kinetic current density at 0.9 V (figure 3.8).

Figure 3.3a shows the voltammograms of $CoPt_3$/carbon NPs of various sizes. As the size of NPs increases from 3 nm to 9 nm, the H_{upd} region (0.05 V < E < 0.4 V vs. RHE) shrinks, resulting in the decrease of specific surface area from 692 to 277 cm^2/mg_{Pt} (figure 3.3b). Specific activities (at 0.9 V vs. RHE) measured with a rotation rate of 1600 rpm and a scan rate of 20 mV/s are also depicted in figure 3.3b, showing an ascending trend as the NP size increases. The specific activity of 9 nm $CoPt_3$/carbon is over two times higher than measured for 3 nm $CoPt_3$/carbon NPs. The two opposite trends in specific surface area and specific activity lead to a volcano-shape behavior in size-dependent mass activities, as shown in figure 3.3c, and therefore, the maximum mass activity has been observed for 4.5 nm Pt_3Co NPs.

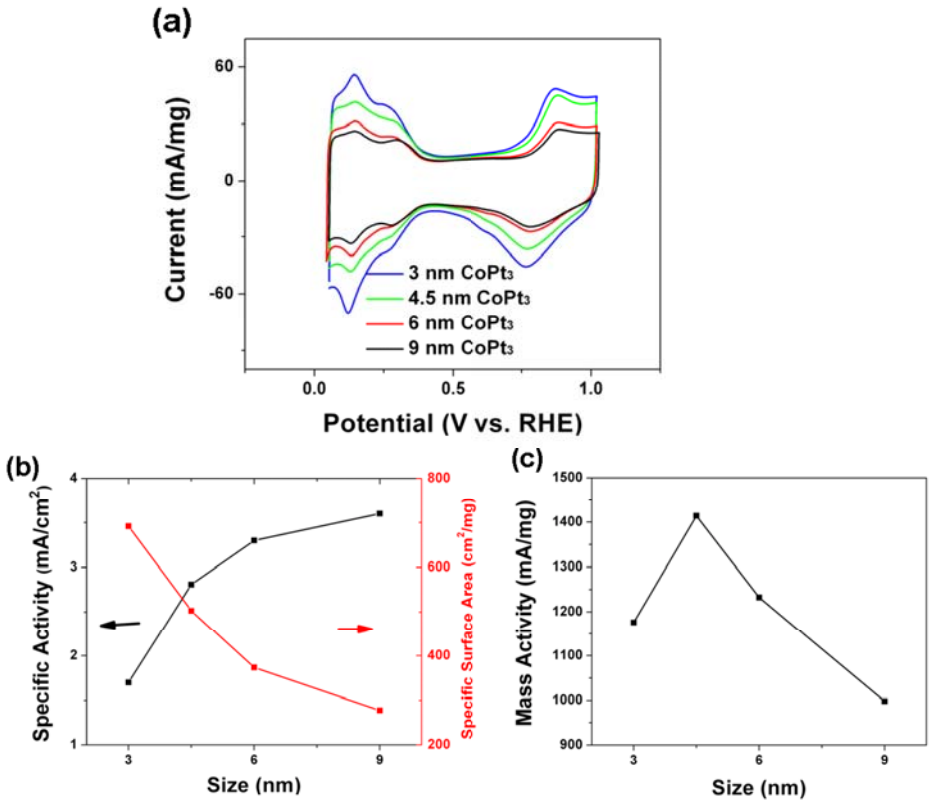

Figure 3.3. (a) CVs of $CoPt_3$ NPs of different sizes. (b) Specific activities at 0.9 V vs. RHE are measured with a scan rate of 20 mV/s and rotation rate of 1600 rpm (black); and specific surface areas (red) of $CoPt_3$/carbon catalysts. The error of specific activities was estimated to be in ±10% according to 3 measurements for each sample. (c) Mass activities of $CoPt_3$/carbon catalysts.

Even though particle size effect for the Pt catalyst has been well documented in literature [22-27], and explained in terms of the surface geometry and associated electronic properties, disputations yet exist. For example, Watanabe *et al.* claim no size effect observed in their combinational electrochemical and ^{195}Pt EC-NMR study. [36] Despite a lack of consensus, it is generally accepted that the mechanism of the Pt size effect is fulfilled through enhanced adsorption of oxygenated species (O^- and OH_{ads}, etc.) in smaller particles, due to the decrease of average coordination number [26], and consequently more pronounced oxophilic behavior. Oxygenated species adsorbed on low-coordinated Pt surface sites (steps, edges, kinks) inhibit the ORR. [23] The first systematic study of bimetallic alloy particles presented here shows that particle size effect is also reflected in the case of $CoPt_3$ NPs. A careful

analysis of the voltammograms presented in figure 3.3a shows that both the oxidation peak (~ 0.9 V) in the anodic scan and the reduction peak (~ 0.8 V) in the cathodic scan exhibit a negative shift of ~30 mV from 9 to 3 nm $CoPt_3$. Our experiments indicate that the smaller NPs are oxidized at lower potential, which corresponds to enhanced adsorption of oxygenated species and thus decreased ORR activity.

The results presented here show about 3-fold enhancement in the ORR (figure 3.4 and table 3.1) between synthesized $CoPt_3$/carbon (6 nm) and commercially available Pt/carbon (6 nm) catalysts. The enhancement has been ascribed to the modification of the Pt surface electronic structure by alloying with 3*d* transition metals. [37-39] The improvement factor is in line with that observed for extended surfaces, [13] implying that the synthetic approach and treatment procedures developed here do produce a homogeneous alloy and highly active monodisperse catalysts with controllable size. Compared with Pt alloy catalysts prepared by conventional approaches such as impregnation and co-precipitation [15-19, 24], the improved activity for Pt-bimetallic NPs developed here is due to the unique chemical solution synthesis, which generates alloy nanoparticles with more homogeneous elemental distribution and better mixing of alloying components, which was found to be crucial in determining the electronic/adsorption/catalytic properties. [12, 13]

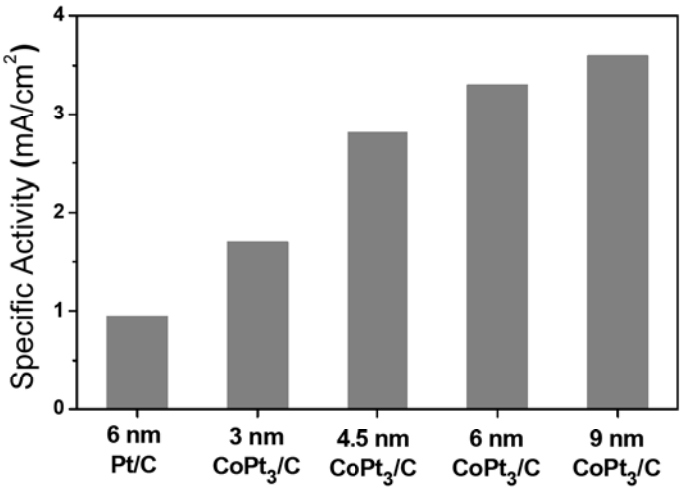

Figure 3.4. Specific activity at 0.9 V vs. RHE, 60^{0}C and 1600 rpm for $CoPt_3$/carbon catalysts compared to 6 nm Pt/carbon catalysts.

3.4 Conclusion

In summary, we have synthesized size controlled monodisperse $CoPt_3$ nanoparticles ranging from 3 nm to 9 nm, and applied them as electrocatalysts for the oxygen reduction reaction. The organic solvothermal approach has proven to be a powerful method for synthesis of high-quality alloy nanoparticles with superior performance in catalyzing the cathodic fuel cell reaction. Systematic study of the Pt-bimetallic alloy catalysts comprising nanoparticles of various sizes reveals that the ORR activity of $CoPt_3$ is size-dependent and decreases with the particle size. By balancing the specific surface area and activity, the optimal size for the maximum in mass activity was established to be around 4.5 nm. In a quest to control the size, shape, and composition of nanoparticles, the strategy and trends reported in this study may be generalized to other systems and utilized to guide the future development of advanced functional nanomaterials.

3.5 Appendix

3.5.1 Synthesis of Pt_3Co nanoparticles

In a typical synthesis of 4.5 nm Pt_3Co NPs, 0.16 mmol $Pt(acac)_2$ was dissolved in 10 ml oleylamine and 5 ml benzyl ether, in the presence of 1 mmol 1-tetradecanediol, 2.8 mmol 1-adamantanecarboxylic acid. The formed solution was heated to 200 ^{o}C under Ar flow. 0.25 mmol cobalt carbonyl dissolved in 1 ml dichlorobenzene was added into this hot solution under the Ar atmosphere. After 30 minutes, the solution temperature was raised to 260 ^{o}C and kept in reflux for 30 minutes. After the reaction, the solution was cooled down to room temperature. 40 ml iso-propanol and 20 ml ethanol were added to precipitate NPs, followed by centrifuge (6500 rpm, 6 minutes). The collected product was dispersed in 10 ml hexane for further applications. Electrochemical properties of synthesized NPs were compared to the commercially available state-of-the-art Pt/carbon catalyst supplied by Tanaka.

3.5.2 Characterization

The TEM images (figure 3.1) and EDX spectrum (figure 3.5) were collected on a Philips CM 30 TEM equipped with EDX functionality. The EDX analysis covered a large area of the nanoparticle assembly (> 1 μm × 1μm, over thousands of particles). XRD patterns (figure 3.2) were collected on a Rigaku RTP 300 RC machine. Crystalline size in the NPs were calculated by the Scherrer equation for the (111) peak after background correction of the spectrum (0.94 was used for the Scherrer constant).

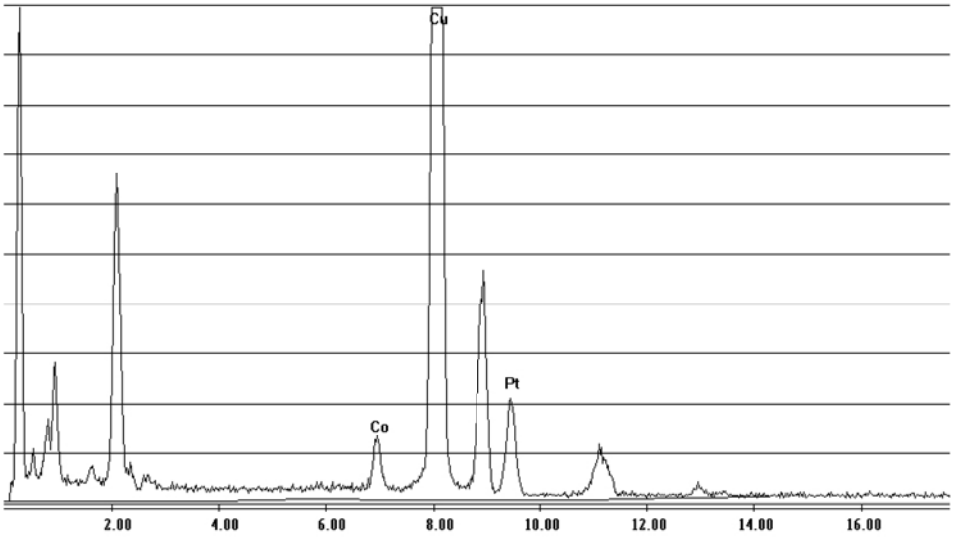

Figure 3.5. EDX spectrum of Pt3Co NPs confirming the atomic ratio between Co and Pt is equal to 1:3.

3.5.3 Electrochemical Measurements

The electrochemical measurements were conducted in a three-compartment electrochemical cell with a rotating disc electrode setup (Pine) and potentiostat (Ecochemie Autolab 302). A saturated Ag/AgCl electrode and a Pt wire were used as reference and counter electrodes, respectively. 0.1 M $HClO_4$ was used as electrolyte. Details about sample preparation and loading were presented in the text.

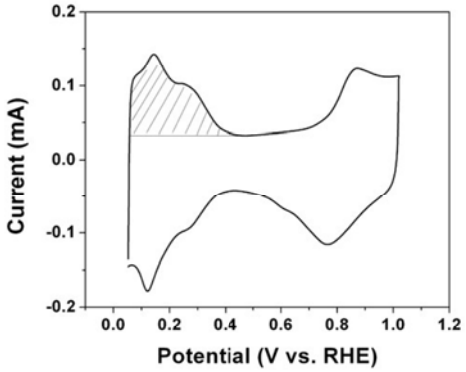

Figure 3.6. CV of 3 nm Pt_3Co/carbon catalyst measured at 50 mV s^{-1}. The electrochemically active surface area of the catalyst can be obtained by $S = \frac{Q_s}{200 \ \ \mu C \cdot cm^{-2}}$, where Qs is the surface charge that can be calculated from the area under the Hupd peak by $Q_s = \frac{\int I \cdot dE}{\nu}$, where *v* is the scan rate.

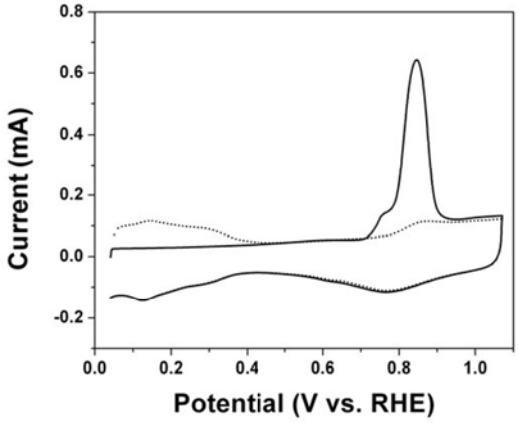

Figure 3.7. CO stripping of 3 nm Pt_3Co/carbon catalyst measured at 50 mV s^{-1}. The dashed curve is the blank CV recorded right after CO stripping. The coverage of CO calculated by $\Theta_{CO} = \frac{\frac{1}{2}Q_{CO}}{Q_{H_{upd}}}$ is 94%.

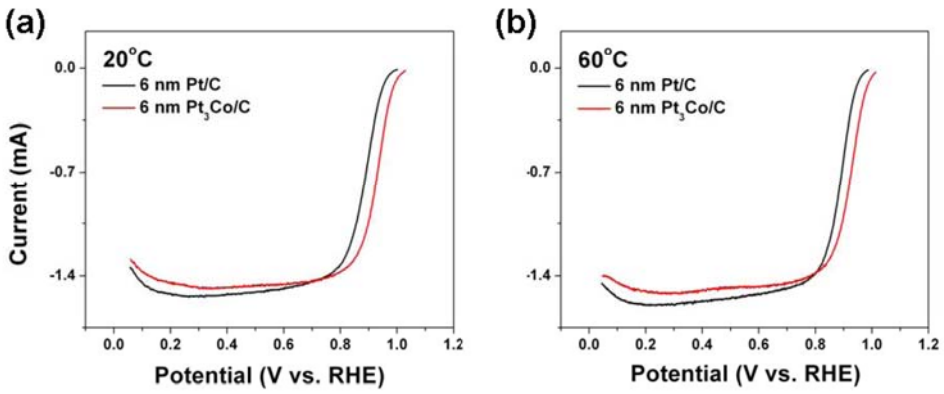

Figure 3.8. Polarization curves for 6 nm Pt and Pt_3Co/carbon catalysts measured at (a) 20°C and (b) 60°C with 20 mV s^{-1} at 1600 rpm. Kinetic current density was obtained by $\frac{1}{I} = \frac{1}{I_k} + \frac{1}{I_{diff}}$. $J_k = \frac{I_k}{surface\ \ area}$**,where the *surface area* was obtained from the CV as shown in figure 3.6 and CO stripping curve in figure 3.7.**

Table 3.1. Summary of electrochemical measurements for Pt and Pt_3Co/carbon catalysts.

NPs	Loading ($\mu g_{Pt}/cm^2_{disk}$)	Surface Area (cm^2)	Specific Activity at 0.9 V vs. RHE (mA/cm^2)	Mass Activity at 0.9 V vs. RHE (mA/mg_{Pt})
3 nm Pt_3Co	9	1.848	1.62	1176
4.5 nm Pt_3Co	9	1.344	2.68	1414
6 nm Pt_3Co	9	0.998	3.14	1233
9 nm Pt_3Co	12	0.987	3.43	998
6 nm Pt	9	0.981	0.97	374

References

[1] S. H. Sun, C. B. Murray, D. Weller, L. Folks, and A. Moser, Science 287 (2000) 1989.

[2] C. Desvaux, C. Amiens, P. Fejes, P. Renaud, M. Respaud, P. Lecante, E. Snoeck, and B. Chaudret, Nature Materials 4 (2005) 750.

[3] S. D. Bader, Reviews of Modern Physics 78 (2006) 1.

[4] W. S. Seo, J. H. Lee, X. M. Sun, Y. Suzuki, D. Mann, Z. Liu, M. Terashima, P. C. Yang, M. V. McConnell, D. G. Nishimura, and H. J. Dai, Nature Materials 5 (2006) 971.

[5] C. Wang, S. Peng, L. M. Lacroix, and S. H. Sun, Nano Research 2:380 (2009).

[6] S. Link, Z. L. Wang, and M. A. El-Sayed, Journal of Physical Chemistry B 103 (1999) 3529.

[7] E. Cottancin, J. Lerme, M. Gaudry, M. Pellarin, J. L. Vialle, M. Broyer, B. Prevel, M. Treilleux, and P. Melinon, Physical Review B 62 (2000) 5179.

[8] Y. G. Sun, B. Wiley, Z. Y. Li, and Y. N. Xia, Journal of the American Chemical Society 126 (2004) 9399.

[9] C. Wang, S. Peng, R. Chan, and S. H. Sun, Small 5 (2009) 567.

[10] T. Toda, H. Igarashi, H. Uchida, and M. Watanabe, Journal of the Electrochemical Society 146 (1999) 3750.

[11] J. Greeley and M. Mavrikakis, Nature Materials 3 (2004) 810.

[12] V. R. Stamenkovic, B. Fowler, B. S. Mun, G. F. Wang, P. N. Ross, C. A. Lucas, and N. M. Markovic, Science 315 (2007) 493.

[13] V. R. Stamenkovic, B. S. Mun, M. Arenz, K. J. J. Mayrhofer, C. A. Lucas, G. F. Wang, P. N. Ross, and N. M. Markovic, Nature Materials 6 (2007) 241.

[14] C. Wang, H. G. Yin, R. Chan, S. Peng, S. Dai, and S. H. Sun, Chemistry of Materials 21 (2009) 433.

[15] E. Blomsma, J. A. Martens, and P. A. Jacobs, Journal of Catalysis 165 (1997) 241.

[16] J. R. C. Salgado, E. Antolini, and E. R. Gonzalez, Journal of Power Sources 141 (2005) 13.

[17] Y. D. Qian, W. Wen, P. A. Adcock, Z. Jiang, N. Hakim, M. S. Saha, and S. Mukerjee, Journal of Physical Chemistry C 112 (2008) 1146.

[18] N. H. H. Abu Bakar, M. M. Bettahar, M. Abu Bakar, S. Monteverdi, J. Ismail, and M. Alnot, Journal of Molecular Catalysis a-Chemical 308 (2009) 87.

[19] M. Neergat, A. K. Shukla, and K. S. Gandhi, Journal of Applied Electrochemistry 31 (2001) 373.

[20] J. N. Soderberg, A. H. C. Sirk, S. A. Campbell, and V. I. Birss, Journal of the Electrochemical Society 152 (2005) A2017.

[21] M. A. García-Contreras, S. M. Fernández-Valverde, and J. R. Vargas-García, Journal of Alloys and Compounds 434-435 (2007) 522.

[22] K. Kinoshita, Journal of the Electrochemical Society 137 (1990) 845.

[23] K. J. J. Mayrhofer, B. B. Blizanac, M. Arenz, V. R. Stamenkovic, P. N. Ross, and N. M. Markovic, Journal of Physical Chemistry B 109 (2005) 14433.

[24] H. A. Gasteiger, S. S. Kocha, B. Sompalli, and F. T. Wagner, Applied Catalysis B-Environmental 56 (2005) 9.

[25] C. Wang, H. Daimon, T. Onodera, T. Koda, and S. H. Sun, Angewandte Chemie-International Edition 47 (2008) 3588.

[26] B. C. Han, C. R. Miranda, and G. Ceder, Physical Review B 77 (2008) 075410.

[27] C. K. Tsung, J. N. Kuhn, W. Y. Huang, C. Aliaga, L. I. Hung, G. A. Somorjai, and P. D. Yang, Journal of the American Chemical Society 131 (2009) 5816.
[28] M. K. Min, J. H. Cho, K. W. Cho, and H. Kim, Electrochimica Acta 45 (2000) 4211.
[29] Q. S. Liu, Z. Yan, N. L. Henderson, J. C. Bauer, D. W. Goodman, J. D. Batteas, and R. E. Schaak, Journal of the American Chemical Society 131 (2009) 5720.
[30] E. V. Shevchenko, D. V. Talapin, A. L. Rogach, A. Kornowski, M. Haase, and H. Weller, Journal of the American Chemical Society 124 (2002) 11480.
[31] E. V. Shevchenko, D. V. Talapin, H. Schnablegger, A. Kornowski, O. Festin, P. Svedlindh, M. Haase, and H. Weller, Journal of the American Chemical Society 125 (2003) 9090.
[32] B. L. Cushing, V. L. Kolesnichenko, and C. J. O'Connor, Chemical Reviews 104 (2004) 3893.
[33] H. F. Yin, C. Wang, H. G. Zhu, S. H. Overbury, S. H. Sun, and S. Dai, Chemical Communications (2008) 4357.
[34] Z. F. Liu, M. Shamsuzzoha, E. T. Ada, W. M. Reichert, and D. E. Nikles, Journal of Power Sources 164 (2007) 472.
[35] J. Newman, Journal of the Electrochemical Society 113 (1966) 501.
[36] H. Yano, J. Inukai, H. Uchida, M. Watanabe, P. K. Babu, T. Kobayashi, J. H. Chung, E. Oldfield, and A. Wieckowski, Physical Chemistry Chemical Physics 8 (2006) 4932.
[37] J. Greeley, J. K. Norskov, and M. Mavrikakis, Annual Review of Physical Chemistry 53 (2002) 319.
[38] J. L. Zhang, M. B. Vukmirovic, Y. Xu, M. Mavrikakis, and R. R. Adzic, Angewandte Chemie-International Edition 44 (2005) 2132.
[39] V. Stamenkovic, B. S. Mun, K. J. J. Mayrhofer, P. N. Ross, N. M. Markovic, J. Rossmeisl, J. Greeley, and J. K. Norskov, Angewandte Chemie-International Edition 45 (2006) 2897.
[40] Chapter 2 of this thesis.